Kim and Auh *Applied Biological Chemistry* (2026) 69:37
https://doi.org/10.1186/s13765-026-01107-z

KSABC
The Korean Society for Applied Biological Chemistry

ARTICLE Open Access

Protective effects of *Aruncus dioicus* leaf extract against dexamethasone-induced muscle atrophy in C2C12 myotubes

Kyoung Bin Kim[1] and Joong-Hyuck Auh[1*]

Abstract
Dexamethasone-induced muscle atrophy, characterized by excessive protein degradation and increased oxidative stress, represents a significant clinical challenge in patients undergoing long-term glucocorticoid therapy. Natural polyphenols have garnered increasing attention as promising therapeutic agents due to their antioxidant and anti-atrophic properties. This study investigated the protective effects of *Aruncus dioicus* leaf extract and its preparative fractions against dexamethasone-induced muscle atrophy in differentiated C2C12 myotubes. A 70% ethanolic extract was fractionated using preparative HPLC into two distinct fractions, F1 and F2. Phytochemical analysis revealed that F2 exhibited the highest total phenolic content, total flavonoid content, and strongest antioxidant capacity, as determined by both DPPH and ORAC assays, among all tested samples. Pretreatment with F2 significantly attenuated dexamethasone-induced myotube atrophy by preserving myotube diameter, reducing intracellular reactive oxygen species (ROS) levels, and suppressing the upregulation of the muscle-specific ubiquitin ligases muscle atrophy F-box (MAFbx) and muscle RING finger 1 (MuRF1). UHPLC–Orbitrap MS/MS analysis demonstrated that F2 was enriched in flavonol glycosides and phenolic acids. These findings suggest that the F2 fraction of *A. dioicus*, which is rich in bioactive polyphenols, protects against dexamethasone-induced muscle atrophy by suppressing oxidative stress and atrogene expression.

Keywords Antioxidant, *Aruncus dioicus*, C2C12 myotubes, dexamethasone, flavonoid glycosides, muscle atrophy, polyphenols, UHPLC–Orbitrap MS/MS, ubiquitin ligase

Introduction

Aruncus dioicus, a traditional wild edible plant belonging to the family Rosaceae, is native to East Asia and has been consumed both as food and as a folk remedy for centuries [1]. It is typically consumed as blanched young shoots composed of tender stems and expanding leaves. Previous studies have reported that *A. dioicus* extracts exhibit antioxidant and metabolic regulatory activities, and have suggested additional bioactive properties, including anti-inflammatory, anti-obesity, and anti-diabetic effects, supporting its potential as a valuable source of phytochemicals with physiological benefits [1–3].

Skeletal muscle atrophy is characterized by impaired anabolic signaling and enhanced catabolic pathways [4]. A well-established hallmark of atrophic signaling is activation of the ubiquitin-proteasome system (UPS), accompanied by increased expression of the muscle-specific E3 ubiquitin ligases muscle atrophy F-box (MAFbx, also known as Atrogin-1) and muscle RING finger 1 (MuRF1), which are largely regulated by forkhead box O

*Correspondence:
Joong-Hyuck Auh
jhauh@cau.ac.kr
[1]Department of Food Science and Biotechnology, Chung-Ang University, Anseong 17546, Republic of Korea

© The Author(s) 2026. **Open Access** This article is licensed under a Creative Commons Attribution 4.0 International License, which permits use, sharing, adaptation, distribution and reproduction in any medium or format, as long as you give appropriate credit to the original author(s) and the source, provide a link to the Creative Commons licence, and indicate if changes were made. The images or other third party material in this article are included in the article's Creative Commons licence, unless indicated otherwise in a credit line to the material. If material is not included in the article's Creative Commons licence and your intended use is not permitted by statutory regulation or exceeds the permitted use, you will need to obtain permission directly from the copyright holder. To view a copy of this licence, visit http://creativecommons.org/licenses/by/4.0/.

Springer

(FoxO) transcription factors [5]. Under anabolic conditions, phosphoinositide 3-kinase (PI3K)/protein kinase B (Akt)/mechanistic target of rapamycin (mTOR) signaling phosphorylates FoxO proteins, retaining them in the cytoplasm and thereby suppressing atrophy-related gene expression [5]. In contrast, suppression of this pathway promotes FoxO nuclear translocation and upregulation of atrophy-associated genes, thereby accelerating proteolysis [6]. In many catabolic conditions, oxidative stress and the accumulation of reactive oxygen species (ROS) further contribute to proteolytic signaling and contractile dysfunction [7].

Dexamethasone (DEX), a synthetic glucocorticoid, is widely used to induce muscle atrophy in both in vitro and in vivo models [8]. In differentiated myotubes, DEX activates glucocorticoid receptor–dependent catabolic programs that attenuate insulin-like growth factor-1 (IGF-1)–Akt–mTOR signaling and promote FoxO nuclear translocation. This process leads to upregulation of MAFbx and MuRF1 and subsequent enhancement of UPS-mediated protein degradation [9]. DEX treatment has also been associated with elevated oxidative stress and increased ROS production, suggesting that redox imbalance is an important contributor to glucocorticoid-induced muscle wasting [10, 11].

Diet-derived polyphenols have attracted considerable attention for their potential to counteract muscle atrophy, largely due to their antioxidant and anti-inflammatory properties, as well as their capacity to modulate muscle protein turnover pathways [12, 13]. In experimental models, various polyphenols have been shown to suppress the upregulation of MAFbx and MuRF1, restore Akt-mediated anabolic signaling, and reduce oxidative stress, thereby attenuating myotube atrophy [14]. In particular, polyphenols and flavonoids are gaining attention as natural compounds with potential relevance to muscle health. Their structural diversity, wide availability, and relatively favorable toxicological profiles support their further investigation in experimental models [14].

Despite these advances, the potential role of *A. dioicus*-derived phytochemicals in glucocorticoid-induced muscle atrophy remains largely unexplored. Therefore, in this study, a 70% ethanolic extract of *A. dioicus* leaves (ADL) was prepared and further fractionated into two phenolic fractions, Fraction 1 (F1) and Fraction 2 (F2), using preparative chromatography. Using differentiated C2C12 myotubes challenged with DEX, we evaluated the anti-atrophic effects of ADL, F1, and F2 by assessing morphological indicators of atrophy, cell viability, and the expression of key atrophy markers, MAFbx and MuRF1. The antioxidant capacities of these preparations were characterized through phytochemical profiling and radical-scavenging assays. This study aimed to evaluate the anti-atrophic potential of ADL-derived fractions in dexamethasone-induced C2C12 myotubes and to characterize their chemical and biological properties for further validation.

Results

Preparation of *Aruncus dioicus* extract and fractions

Freeze-dried *A. dioicus* leaves were extracted with 70% aqueous ethanol, yielding 32.10 ± 0.03% (w/w) crude extract based on dry weight. Preparative high-performance liquid chromatography (HPLC) fractionation of ADL produced two major fractions, F1 and F2, according to their UV chromatographic profiles (Fig. 1). F1 (retention time 2–12 min) was recovered with a yield of 45.77 ± 1.22% and exhibited a reddish appearance. F2 (retention time 12–25 min) was obtained with a yield of 28.53 ± 0.91% and displayed a distinct yellow coloration.

Phytochemical content and antioxidant activities

The phytochemical contents of crude ADL and its preparative fractions (F1 and F2) are presented in Table 1. Among the tested samples, F2 consistently exhibited the highest total phenolic content (TPC, 437.79 ± 8.89 mg gallic acid equivalents (GAE)/g) and total flavonoid content (TFC, 324.48 ± 1.94 mg quercetin equivalents (QE)/g). These values were significantly higher in F2 than in crude ADL (TPC: 220.48 ± 0.95 mg GAE/g; TFC: 154.73 ± 1.56 mg QE/g) and F1 (TPC: 108.84 ± 0.81 mg GAE/g; TFC: 79.51 ± 0.78 mg QE/g) ($p < 0.05$).

Antioxidant capacity was evaluated using the DPPH radical-scavenging assay and the oxygen radical absorbance capacity (ORAC) assay (Table 1). In the DPPH assay, F2 demonstrated the strongest radical-scavenging activity, as indicated by the lowest half-maximal inhibitory concentration (IC_{50}) value (18.01 ± 1.75 μg/mL), which was significantly lower than that of crude ADL (23.60 ± 1.50 μg/mL) and F1 (59.86 ± 3.37 μg/mL) ($p < 0.05$). Lower IC_{50} values indicate stronger antioxidant activity. Consistent with these findings, the ORAC assay showed that F2 exhibited the highest antioxidant capacity (4841.46 ± 103.05 μM Trolox equivalents (TE)/mg), substantially exceeding crude ADL (3125.80 ± 116.13 μM TE/mg) and F1 (2059.52 ± 94.08 μM TE/mg) ($p < 0.05$).

Cytotoxicity of ADL fractions in C2C12 cell

To assess cytotoxicity, differentiated C2C12 myotubes were pretreated with ADL or its fractions for 24 h on day 3 of differentiation, followed by dexamethasone treatment for 24 h on day 4. Cell viability was then evaluated at concentrations of 30, 50, and 100 μg/mL. Crude ADL and F1 maintained cell viability above 80% at all tested concentrations. For F2, cell viability remained above 90% at 30 and 50 μg/mL but decreased to below

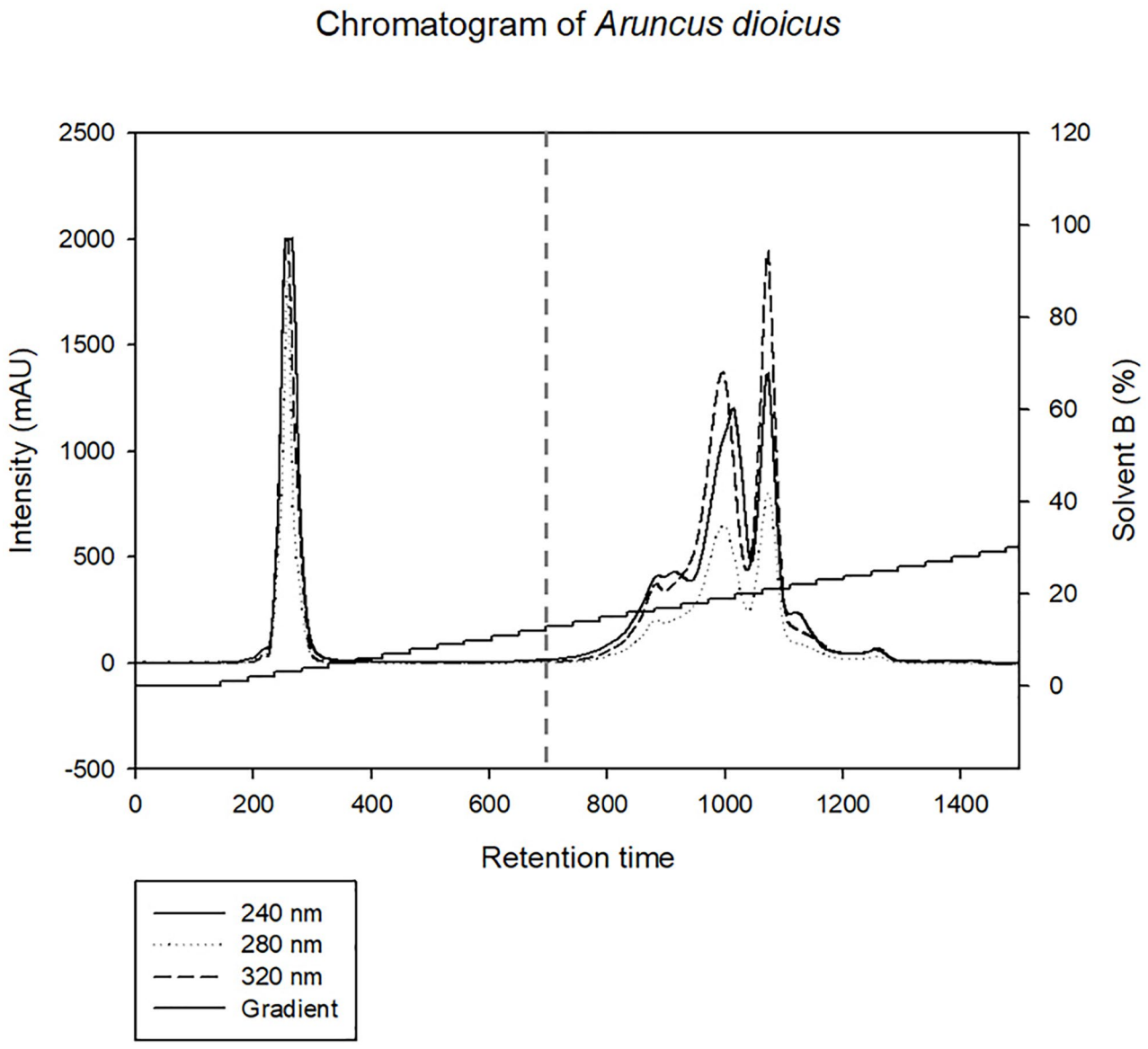


Fig. 1 Preparative chromatogram of *Aruncus dioicus* leaf extract. The crude extract was separated into two major fractions (F1 and F2), as indicated by the vertical dashed lines. Separation was monitored using multi-wavelength UV detection at 240 nm (solid line), 280 nm (dotted line), and 320 nm (dashed line). The secondary y-axis represents the gradient profile of Solvent B (%)

Table 1 Total phenolic and flavonoid contents and antioxidant activities of *Aruncus dioicus* leaf extract and its fractions

Sample	Total phenolic content (mg of GAE/g of sample)	Total flavonoid content (mg of QE/g of sample)	DPPH IC_{50} (μg/mL)	ORAC (μM TE/mg)
Crude	220.48 ± 0.95^{b}	154.73 ± 1.56^{b}	23.60 ± 1.50^{b}	3125.80 ± 116.13^{b}
F1	108.84 ± 0.81^{c}	79.51 ± 0.78^{c}	59.86 ± 3.37^{a}	2059.52 ± 94.08^{c}
F2	437.79 ± 8.89^{a}	324.48 ± 1.94^{a}	18.01 ± 1.75^{c}	4841.46 ± 103.05^{a}

Values are expressed as mean ± SD of three independent biological replicates. Different lowercase letters within the same column indicate statistically significant differences ($p < 0.05$). GAE, gallic acid equivalents; QE, quercetin equivalents; TE, Trolox equivalents; IC_{50}, half-maximal inhibitory concentration; ORAC, oxygen radical absorbance capacity; DPPH, 2,2-diphenyl-1-picrylhydrazyl

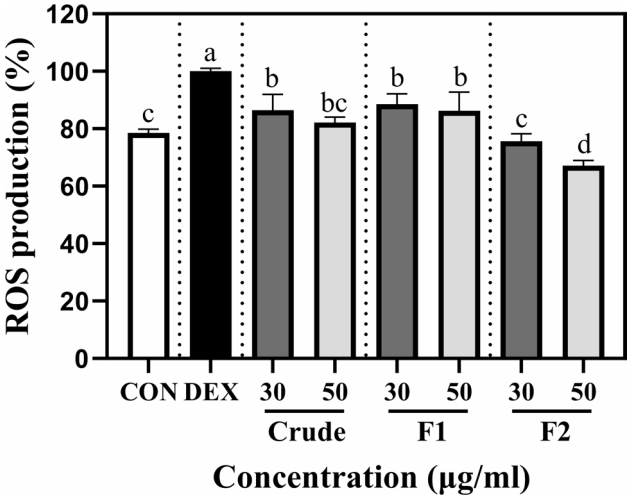


Fig. 2 Inhibition of dexamethasone (DEX)-induced ROS production by *Aruncus dioicus* leaf extract and its fractions. Cells were treated with DEX (10 μM) in the presence or absence of crude extract, Fraction 1 (F1), or Fraction 2 (F2) at 30 and 50 μg/mL. ROS production is expressed as a percentage relative to the DEX-treated group (100%). Data are presented as mean ± SD from three independent biological replicates. Different lowercase letters indicate statistically significant differences ($p < 0.05$) determined by one-way ANOVA followed by Duncan's multiple range test

80% at 100 μg/mL. Based on these results, concentrations of 50 μg/mL or lower were selected for subsequent experiments.

Inhibition of intracellular ROS accumulation

The effects of ADL and its fractions on intracellular ROS production were evaluated in C2C12 myotubes treated with dexamethasone (Fig. 2). DEX treatment significantly increased ROS accumulation compared with the control group. Pretreatment with F2 at 50 μg/mL reduced DEX-induced ROS levels by 33%, representing a significant attenuation of oxidative stress. In contrast, crude ADL and F1 exhibited comparatively weaker ROS-suppressing effects than F2.

Myotube morphology and atrogene expression

To evaluate the protective effects of the ADL fractions against DEX-induced muscle atrophy, morphological changes in C2C12 myotubes were assessed by immunofluorescence staining (Fig. 3A). DEX treatment induced characteristic atrophic features, including a marked reduction in myotube diameter compared with the untreated control group. Quantitative analysis showed that myotube diameter was significantly reduced in the DEX-treated group (17.70 ± 0.47 μm) relative to the control group (23.01 ± 0.98 μm). Pretreatment with crude ADL, F1 and F2 increased the diameter to 21.56 ± 0.58 μm, 19.89 ± 1.62 μm and 22.52 ± 1.16 μm, respectively. Among the tested samples, F2 most effectively attenuated DEX-induced myotube atrophy and restored myotube diameter to a level not significantly different from that of the untreated control, while crude ADL showed a moderate protective effect. In contrast, F1 produced only limited recovery, with myotube diameter remaining significantly lower than that of the control group (Fig. 3B, $p < 0.05$).

At the molecular level, western blot analysis demonstrated that DEX treatment markedly upregulated

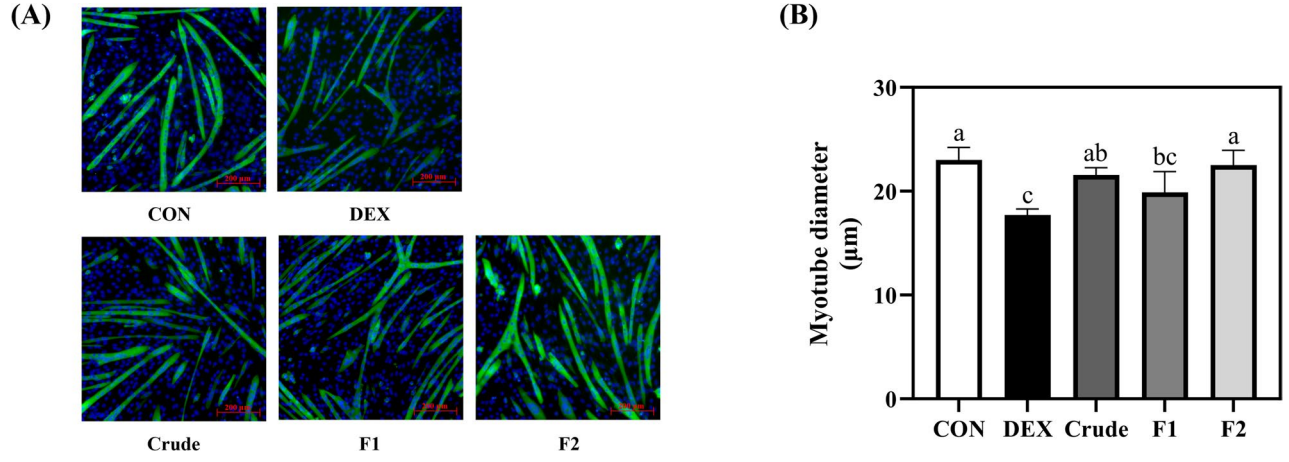


Fig. 3 Protection against dexamethasone (DEX)-induced atrophy by *Aruncus dioicus* leaf extract fractions. (**A**) Representative immunofluorescence images of C2C12 myotubes. Differentiated myotubes were pretreated with crude extract, Fraction 1 (F1), or Fraction 2 (F2) at 30 μg/mL for 24 h, followed by exposure to dexamethasone (10 μM) for an additional 24 h. Myosin heavy chain was stained with an Alexa Fluor 488-conjugated MF20 antibody (green), and nuclei were counterstained with DAPI (blue). DEX treatment induced significant thinning and fragmentation of myotubes, which were markedly attenuated by F2 pretreatment. (**B**) Quantitative analysis of myotube diameter. For each biological replicate, 50 myotubes were measured per treatment group using ImageJ software. Thus, a total of 150 myotubes were analyzed per treatment group across three independent biological replicates. Data are presented as mean ± SD from three independent biological replicates. Different lowercase letters indicate statistically significant differences ($p < 0.05$) determined by one-way ANOVA followed by Duncan's multiple range test

the protein expression of the muscle-specific E3 ubiquitin ligases MAFbx and MuRF1 compared to the untreated control (Fig. 4). Pretreatment with ADL fractions attenuated the expression of both atrogenes in a fraction-dependent manner. For MAFbx, F2 pretreatment restored protein expression to levels comparable to those of the untreated control, representing significantly greater suppression than that achieved by the crude extract or F1 (Fig. 4B). Similarly, F2 exhibited the strongest inhibitory effect on MuRF1 expression, with levels significantly lower than those observed in the DEX-treated group. In contrast, the crude extract and F1 showed partial but non-significant reductions in MuRF1 expression (Fig. 4C).

UHPLC–orbitrap MS/MS metabolite profiling

UHPLC–Orbitrap MS/MS profiling was performed to characterize metabolic differences among the crude extract, F1, and F2 (Fig. 5A). Multivariate analysis using principal component analysis (PCA) clearly separated the three groups into distinct clusters (PC1: 78.8%; PC2: 8.3%), indicating substantial compositional differences among the fractions (Fig. 5B).

To identify key discriminant metabolites between F1 and F2, orthogonal partial least squares–discriminant analysis (OPLS-DA) was conducted. The S-plot showed discriminant features associated with each fraction (Fig. 6A). Variable importance in projection (VIP) score analysis showed that 56 discriminant features satisfied the selection criteria, and 19 were associated with F2 (Fig. 6B). Among these, six compounds were tentatively identified based on accurate mass and MS/MS fragmentation patterns: kaempferol-3-O-glucoside (*m/z* 447.0937, neutral loss of 162 Da corresponding to a hexose moiety, yielding the kaempferol aglycone ion at *m/z* 284.0332), isoquercetin (*m/z* 463.0888, neutral loss of 162 Da to yield *m/z* 300.0277), kaempferol 3-O-(6"-malonylglucoside) (*m/z* 489.1044, $[M-H-CO_2]^-$, with a neutral loss of 205 Da corresponding to malonyl-hexose after in-source CO_2 elimination from the malonyl moiety, yielding *m/z* 284.0332, kaempferol $[M-H]^-$), tiliroside (*m/z* 593.1308, yielding fragment ions at *m/z* 284.0331/285.0407), kaempferol-3-O-rutinoside (*m/z* 593.1518, showing a neutral loss of 308 Da corresponding to a rutinoside moiety to yield *m/z* 285.0408), and dicaffeoylquinic acid (*m/z* 515.1201, yielding fragment

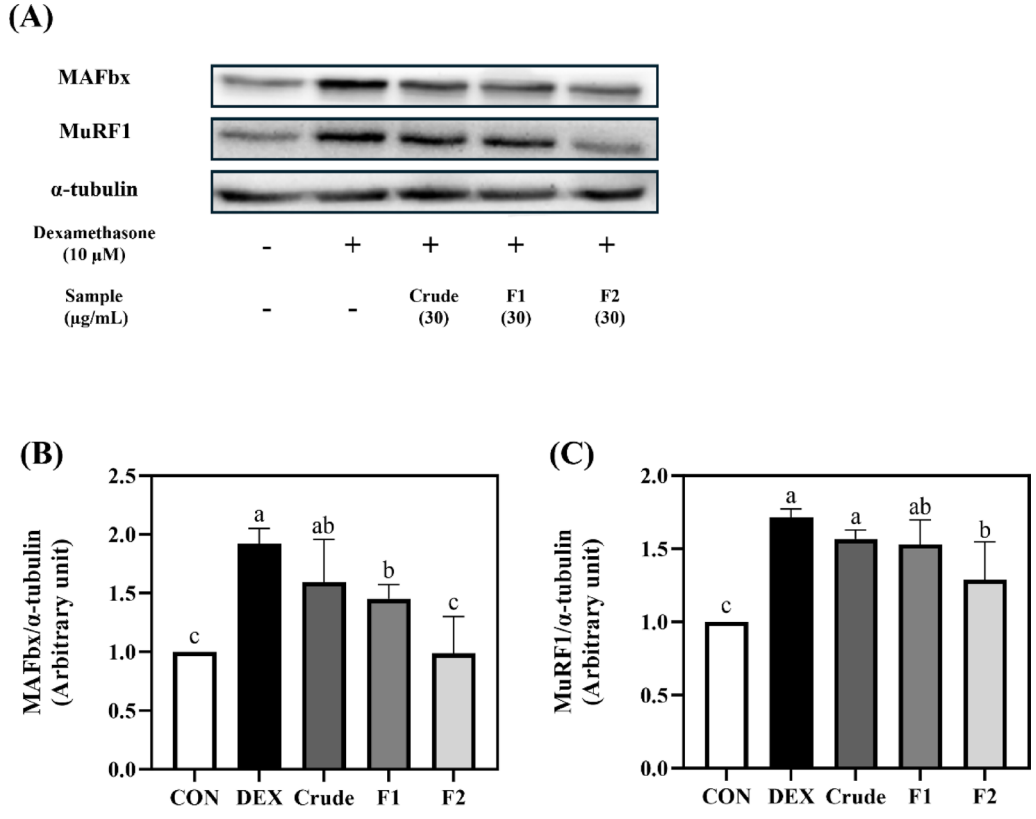


Fig. 4 Suppression of dexamethasone (DEX)-induced ubiquitin ligase expression in C2C12 myotubes by *Aruncus dioicus* leaf extract fractions. (**A**) Representative western blot images of MAFbx, MuRF1, and α-tubulin. (**B**) Relative protein expression levels of MAFbx and (**C**) MuRF1, normalized to α-tubulin. Cells were treated with dexamethasone (10 μM) in the presence or absence of crude extract, Fraction 1 (F1), or Fraction 2 (F2) at 30 μg/mL. Data are presented as mean ± SD from three independent biological replicates. Different letters (**a**–**c**) indicate statistically significant differences among groups ($p < 0.05$) determined by one-way ANOVA followed by Duncan's multiple range test

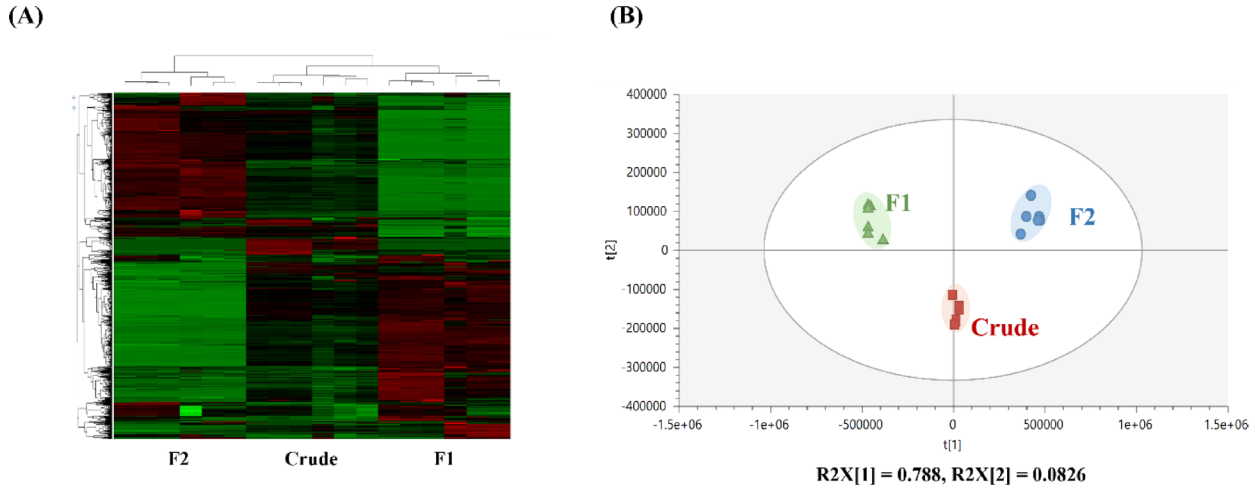


Fig. 5 Metabolite profiling of *Aruncus dioicus* leaf extract and its fractions. (**A**) Heat map showing the relative abundance of metabolites in the crude extract, Fraction 1 (F1), and Fraction 2 (F2). Red and green indicate relatively high and low intensities, respectively. (**B**) Principal component analysis (PCA) score plot showing clear separation among F1 (green triangles), F2 (blue circles), and crude extract (red squares). PC1 and PC2 explain 78.8% and 8.3% of the total variance, respectively. PCA was performed using biological replicate samples ($n = 6$ per group). Each point represents an individual biological replicate

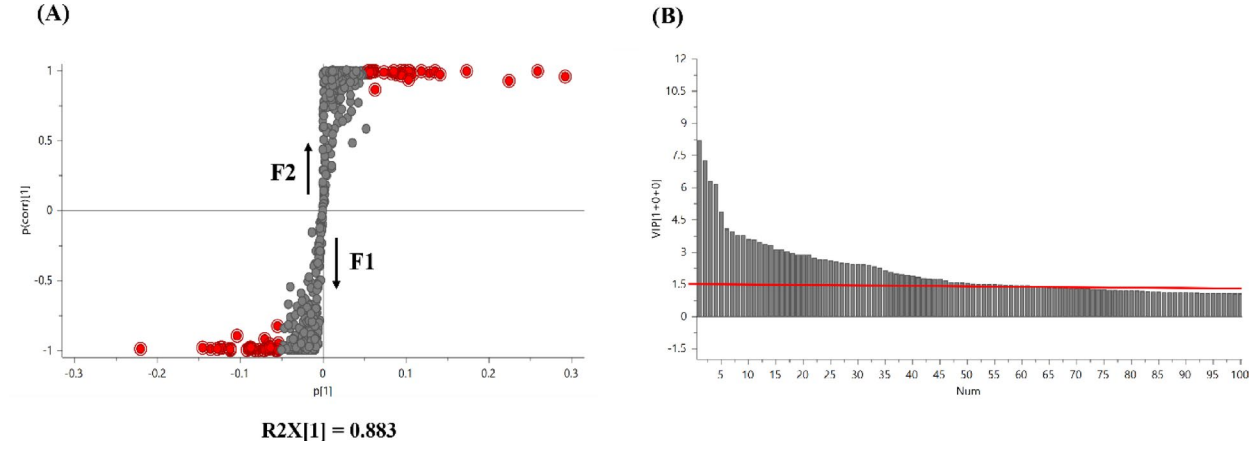


Fig. 6 OPLS-DA analysis of *Aruncus dioicus* leaf extract fractions (F1 and F2). (**A**) OPLS-DA S-plot comparing the metabolic profiles of F1 and F2. Red dots represent significant discriminant features responsible for group separation. Features located in the upper right quadrant are enriched in F2, whereas those in the lower left quadrant are enriched in F1. (**B**) VIP score plot of the top 100 variables among 793 detected ions. The red horizontal line indicates the threshold (VIP = 1.5); 56 features satisfied the criteria of VIP ≥ 1.5 and $p(\text{corr}) \geq 0.95$. OPLS-DA was performed using biological replicate samples ($n = 6$ per fraction)

ions at *m/z* 173.0451/179.0346). The tentatively identified metabolites are summarized (Table 2).

Discussion

This study demonstrated that the F2 fraction of *A. dioicus* effectively mitigates dexamethasone-induced skeletal muscle atrophy in C2C12 myotubes. Preparative LC fractionation successfully concentrated key bioactive secondary metabolites into F2, resulting in a 2.0-fold increase in total phenolic content and a 2.1-fold increase in total flavonoid content compared with the crude extract. The enrichment of these polyphenolic compounds is considered to form the chemical foundation underlying the superior antioxidant and anti-atrophic activities subsequently observed [13, 14].

Prior to evaluating the cellular bioactivity of F2, the antioxidant capacity of each fraction was first assessed using DPPH radical-scavenging and ORAC assays. In both assays, F2 exhibited significantly higher antioxidant activity than the crude extract and F1 (F2 > crude extract > F1), indicating that flavonoid enrichment through preparative fractionation substantially enhanced antioxidant capacity. The DPPH assay measures direct electron-donating capacity against stable radicals, whereas the ORAC assay evaluates protective capacity against oxidative damage induced by peroxyl radicals; thus, these assays provide complementary information. The

Table 2 Tentative identification of discriminant metabolites associated with Fraction 2 of *Aruncus dioicus* leaf extract by UHPLC–Orbitrap MS/MS

m/z	RT (min)	Tentative identification	MS/MS fragment	VIP	*p* (corr)	Error (ppm)
373.1297	9.065	Unknown	259.0615, 179.0710, 153.0552	1.76	0.99	-
389.1457	7.783	Unknown	91.4876, 128.6053, 52.9451	3.62	0.98	-
447.0937	7.845	Kaempferol-3-O-glucoside	284.0332, 255.0302, 227.0350	3.34	1.00	0.92
463.0888	7.554	Isoquercetin	300.0277, 271.0249, 301.0352	2.35	0.98	1.30
487.1252	7.914	Unknown	161.0239, 179.0344, 163.0396	3.81	1.00	-
489.1044	8.05	Kaempferol 3-O-(6″-malonylglucoside) $[M\text{-}CO_2\text{-}H]^-$	284.0332, 285.0407, 255.0303	2.66	1.00	1.13
493.2297	8.808	Unknown	89.0234, 59.0128, 71.0128	2.63	1.00	-
503.1200	7.466	Unknown	161.0239, 179.0346, 135.0445	8.22	0.99	-
503.1200	7.744		161.0239, 179.0346, 135.0445	7.28	1.00	-
503.1204	8.638		161.0237, 179.0344, 135.0443	2.50	0.97	-
505.1722	9.003	Unknown	161.0239, 133.0288, 135.0445	3.05	0.97	-
515.1201	7.98	Dicaffeoylquinic acid	173.0451, 179.0346, 191.0558	2.77	1.00	1.17
517.1353	7.976	Unknown	161.0239, 179.0346, 135.0445	2.90	1.00	-
517.1355	7.888		135.0445, 179.0346, 161.0239	2.09	0.99	-
521.1669	8.434	Unknown	161.0239, 179.0346, 135.0445	4.89	1.00	-
521.1670	8.583		161.0238, 179.0345, 133.0287	2.68	0.97	-
593.1308	8.743	Tiliroside	284.0331, 285.0407, 255.0302	1.54	1.00	1.24
593.1518	7.659	Kaempferol-3-O-rutinoside	285.0408, 284.0332, 255.0303	1.61	0.99	1.02
1043.3412	8.433	Unknown	161.0239, 179.0346, 135.0445	2.41	1.00	-

Metabolites associated with Fraction 2 (F2) were selected from the OPLS-DA model using a VIP threshold ≥ 1.5 and further filtered by *p*(corr) ≥ 0.95, yielding 19 discriminant metabolites. The OPLS-DA model was constructed using biological replicate samples ($n = 6$ per fraction). UHPLC–Orbitrap MS/MS, ultra-high-performance liquid chromatography–Orbitrap tandem mass spectrometry; RT, retention time; VIP, variable importance in projection; OPLS-DA, orthogonal partial least squares–discriminant analysis

consistently superior performance of F2 in both assays suggests that its antioxidant effects are mediated through multiple mechanisms rather than a single mode of action. Moreover, the chemical antioxidant capacity demonstrated in these assays corresponded closely with the suppression of oxidative stress observed at the cellular level, confirming a strong correlation between chemical and biological antioxidant activity [15–17].

At the cellular level, dexamethasone is a synthetic glucocorticoid widely used to model muscle atrophy in vitro, as it induces oxidative stress, disrupts protein homeostasis, and activates catabolic signaling pathways [11, 18, 19]. Although this model does not fully recapitulate the physiological complexity of skeletal muscle in vivo, it remains useful as a preliminary cell-based system for evaluating anti-atrophic candidates. Previous studies using both DEX-treated C2C12 myotubes and DEX-induced mouse models have reported consistent FoxO3-dependent catabolic responses, including oxidative stress and increased expression of atrophy-related markers [16, 20]. In the present study, dexamethasone treatment significantly increased intracellular ROS levels and produced characteristic atrophic phenotypes, including reduced myotube diameter, morphological deterioration, and upregulation of the muscle-specific E3 ubiquitin ligases MAFbx and MuRF1. These ubiquitin ligases are central mediators of muscle protein degradation and are well-established molecular markers of muscle atrophy [21, 22].

F2 suppressed dexamethasone-induced ROS accumulation by 33%, reducing ROS levels to values comparable to or slightly lower than those of the control group. This finding supports the notion that the superior chemical antioxidant capacity confirmed in the DPPH and ORAC assays is effectively translated into the cellular environment [16]. Oxidative stress has been implicated as an important contributor in glucocorticoid-induced muscle atrophy by activating multiple catabolic pathways, including mitochondrial dysfunction, activation of stress-responsive transcription factors such as members of the FoxO family, and subsequent upregulation of atrogenes [18, 23]. In the present study, F2 not only attenuated DEX-induced ROS production but also suppressed the expression of MAFbx and MuRF1. Although the antioxidant activity of F2 is likely associated with its anti-atrophic effects, a direct causal relationship between ROS suppression and atrogene downregulation has not yet been definitively established. Future studies employing specific pathway inhibitors or genetic modulation approaches will be necessary to clarify these mechanistic links [7, 16]. Furthermore, the potential involvement of endogenous antioxidant defense systems, such as the nuclear factor erythroid 2-related factor 2 (Nrf2)/heme oxygenase-1 (HO-1) pathway, requires further investigation. Nonetheless, the present findings clearly demonstrate the strong antioxidant potential of F2 in C2C12 myotubes [16, 24].

The protective effects of F2 extended beyond ROS suppression and were accompanied by reduced protein expression of MAFbx and MuRF1 [5, 19, 25]. A phenotypic hallmark of dexamethasone-induced atrophy in C2C12 myotubes is a reduction in myotube diameter, reflecting enhanced myofibrillar protein degradation [8]. In this study, F2 markedly attenuated the dexamethasone-induced reduction in myotube diameter, indicating preservation of myotube morphology. This morphological protection is consistent with the observed downregulation of the E3 ubiquitin ligases MAFbx and MuRF1, key mediators of ubiquitin–proteasome mediated proteolysis [5]. By suppressing these atrogenes, F2 may reduce excessive proteolytic signaling and thereby contribute to the maintenance of myotube morphology [23]. Collectively, these findings support the anti-atrophic effects of F2 across multiple biological endpoints, including oxidative stress and atrogene expression [25].

The chemical basis underlying the differential biological activities among the fractions was further elucidated through LC–MS/MS-based metabolomic profiling. PCA revealed clear separation among F1, F2, and the crude extract, with PC1 and PC2 explaining 78.8% and 8.3% of the total variance, respectively. To further identify metabolites responsible for the distinct chemical profile of F2, S-plot and VIP score analyses were conducted to compare F1 and F2. Compounds tentatively identified as enriched in F2 included the flavonol glycosides isoquercetin, kaempferol-3-O-glucoside, kaempferol-3-O-rutinoside, tiliroside, and kaempferol 3-O-(6”-malonylglucoside), as well as the phenolic acid di-O-caffeoylquinic acid. The combined presence of these bioactive polyphenols is likely to constitute the molecular basis for the potent antioxidant and anti-atrophic effects observed in F2.

Isoquercetin (quercetin-3-O-glucoside) is a flavonoid with well-documented antioxidant and anti-inflammatory properties [14, 26]. Recent evidence has highlighted its specific role in mitigating skeletal muscle atrophy. For example, isoquercetin has been reported to suppress ROS-mediated oxidative stress and downregulate the expression of atrogenes, including MuRF1 and MAFbx, through activation of the Nrf2/HO-1 signaling pathway [26]. In the present study, the F2 fraction significantly attenuated dexamethasone-induced upregulation of MAFbx and MuRF1 in C2C12 myotubes. This observation is consistent with previous reports demonstrating that quercetin glycosides effectively prevent muscle wasting in dexamethasone-treated murine models [20, 27]. Notably, rutin (quercetin-3-rutinoside) has been shown to inhibit the FoxO3-mediated catabolic program, thereby reducing the induction of muscle-specific E3 ubiquitin ligases [20]. The relatively higher bioavailability and stability of glycosidic forms compared with their aglycone counterparts further support their therapeutic potential in muscle preservation [14, 27].

The F2 fraction was also enriched in multiple kaempferol glycosides, including kaempferol 3-O-glucoside (astragalin), kaempferol 3-O-rutinoside (nicotiflorin), and kaempferol 3-O-(6”-malonylglucoside). Recent studies have highlighted the potent anti-atrophic properties of kaempferol and its glycosidic derivatives in skeletal muscle [28, 29]. Specifically, kaempferol has been shown to protect against dexamethasone-induced muscle atrophy by activating the PI3K/Akt/mTOR signaling pathway while concurrently inhibiting FoxO1 and FoxO3 transcription factors [28]. Moreover, kaempferol has been reported to exert antioxidant effects by modulating the NRF2/HO-1/KEAP1 signaling pathway, thereby attenuating dexamethasone-induced oxidative stress [28].

The presence of diverse glycosidic derivatives may represent muscle-relevant flavonol features associated with metabolic and signaling pathways. For instance, kaempferol 3-O-rutinoside has been reported to promote glucose uptake and increase sirtuin 1 (SIRT1) expression in skeletal muscle cells, thereby improving metabolic homeostasis under stress conditions [29]. Tiliroside, an acylated kaempferol glycoside, has been shown to ameliorate metabolic dysfunction in skeletal muscle through activation of AMPK and adiponectin signaling pathways, further contributing to muscle health maintenance [30].

In addition to flavonoid glycosides, dicaffeoylquinic acid was tentatively identified as a key discriminant phenolic compound in F2. Dicaffeoylquinic acids are well recognized for their strong antioxidant, anti-inflammatory, and hypoglycemic activities [31]. In skeletal muscle contexts, caffeoylquinic acid derivatives such as chlorogenic acid have been reported to attenuate muscle atrophy under various catabolic conditions by modulating oxidative stress and inflammatory signaling pathways [32]. Based on these findings, the dicaffeoylquinic acid identified in F2 may similarly contribute to its anti-atrophic effects, although direct mechanistic evidence in skeletal muscle remains to be established.

The higher phenolic and flavonoid contents, stronger antioxidant capacity, and distinct F2-associated metabolite profile support the description of F2 as an ADL-derived polyphenol-rich fraction with potential anti-atrophic activity in C2C12 myotubes. However, further studies using independently prepared samples, quantitative marker-compound analysis, and purified or isolated compounds are needed to clarify standardization criteria and the contribution of individual metabolites.

In conclusion, preparative HPLC fractionation of ADL yielded an F2 fraction enriched in flavonol glycosides and phenolic acids, including isoquercetin, kaempferol glycosides, tiliroside, and dicaffeoylquinic acid. F2 effectively attenuated dexamethasone-induced muscle atrophy in

C2C12 myotubes and was associated with reduced oxidative stress, decreased MAFbx and MuRF1 expression, and preservation of myotube morphology. These findings provide foundational cell-based evidence supporting the anti-atrophic potential of F2 in DEX-induced C2C12 myotubes. Further in vivo validation and targeted analysis of marker compounds would help confirm its physiological relevance and clarify its applicability as an anti-atrophic candidate.

Materials and methods

Chemicals and reagents

A. dioicus was purchased from a local market in Gangwon-do, South Korea, in 2025. Dulbecco's Modified Eagle Medium (DMEM) and Dulbecco's phosphate-buffered saline (DPBS) were obtained from Biowest (Nuaillé, France). Penicillin–streptomycin, fetal bovine serum (FBS), horse serum (HS), and Trypsin-EDTA (0.05%) were purchased from Gibco (Thermo Fisher Scientific, Waltham, MA, USA). 3-(4,5-dimethylthiazol-2-yl)-2,5-diphenyltetrazolium bromide and dimethyl sulfoxide (DMSO) were obtained from Samcheon Chemical (Pyeongtaek, Korea). A 4% paraformaldehyde solution was purchased from Biosesang (Seongnam-si, Korea). Alexa 488 anti-myosin-4 monoclonal antibody (MF20, 53-6503-82), used for immunofluorescence assays, was purchased from Invitrogen (Waltham, MA, USA). Anti-MuRF1 (sc-398608) and anti-MAFbx (sc-166806) antibodies were obtained from Santa Cruz Biotechnology (Dallas, Texas, USA). α-Tubulin (#DM1A) and anti-mouse IgG-HRP (#7076) secondary antibodies were purchased from Cell Signaling Technology (Danvers, MA, USA). LC-grade methanol for preparative HPLC was obtained from Honeywell (Charlotte, NC, USA). LC/MS-grade acetonitrile, water, and formic acid for LC–MS/MS analysis were purchased from Thermo Fisher Scientific (Waltham, MA, USA).

Sample preparation

A. dioicus leaves were freeze-dried and ground into a fine powder using a blender (SMX-4500PN, Shinil, Korea). A 2 g portion of the dried powder was mixed with 100 mL of 70% ethanol (1:50, w/v) and extracted for 30 min using a bath sonicator (CPX5800H-E sonicator, Branson, MO, USA). Following extraction, the mixture was centrifuged at 12,000 × g for 10 min, and the supernatant was filtered through Whatman No. 1 filter paper (GE Healthcare, UK). The filtrate was concentrated under reduced pressure using a rotary vacuum evaporator (Eyela, Tokyo, Japan) at 36 °C and subsequently lyophilized to obtain a dried extract powder. The dried extract was stored at − 50 °C until further use.

Fractionation of ADL 70% ethanol extracts

Fractionation of the 70% ethanol extract of ADL was performed using a preparative HPLC system (LC-Forte/R, YMC Co., Shimogyo-ku, Japan) equipped with a YMC Triart C18-S column (250 × 15 mm, 20 μm). The mobile phases consisted of distilled water (solvent A) and acetonitrile (solvent B). The flow rate was set at 10 mL/min, and the injection volume was 5 mL (15 mg/mL). The gradient elution program was as follows: 0–2 min, 0% B; 2–25 min, 0–30% B; 25–30 min, 30–100% B; and 30–40 min, 100% B. UV detection was performed at 240, 280, and 320 nm using a diode array detector. Collected fractions were concentrated under reduced pressure using a rotary vacuum evaporator (Eyela) to remove acetonitrile, freeze-dried, and stored at − 50 °C until use.

Measurement of phytochemical content

Total phenolic content

The TPC of ADL and its fractions was determined using the Folin–Ciocalteu method with gallic acid as the standard, with minor modifications [33]. Briefly, 100 μL of sample was mixed with 500 μL of 0.2 M Folin–Ciocalteu reagent and 400 μL of 10% Na_2CO_3. The mixture was incubated at 37 °C for 1 h, and absorbance was measured at 750 nm using a nanophotometer (IMPLEN, München, Germany). Results were expressed as mg GAE per gram of dry weight.

Total flavonoid content

TFC was determined using an $AlCl_3$ colorimetric assay with quercetin as the standard [34]. Briefly, 100 μL of diluted sample was mixed with 400 μL of distilled water. Then, 30 μL of 5% $NaNO_2$ was added, and the mixture was allowed to stand for 5 min. Subsequently, 30 μL of 10% $AlCl_3$ was added, followed by incubation for 6 min. Color development was initiated by adding 200 μL of 1 M NaOH and 240 μL distilled water. Absorbance was measured at 415 nm using a nanophotometer (IMPLEN, München, Germany). Results were expressed as mg QE per gram of dry weight.

Evaluation of antioxidant activity

DPPH radical scavenging activity

DPPH radical-scavenging activity was measured according to a previously described method [35], with minor modifications. A 0.2 mM DPPH solution (2,2-diphenyl-1-picrylhydrazyl; Alfa Aesar, Haverhill, MA, USA) was prepared in methanol (≥ 99.9%), and ascorbic acid was used as the positive control. In a 96-well plate, 200 μL of sample was mixed with 100 μL of 0.2 mM DPPH solution and incubated in the dark at 37 °C for 30 min. Absorbance at 517 nm was measured every 5 min using a microplate reader (SpectraMax M2, Molecular Devices, San Jose, CA, USA). Radical-scavenging activity (%) was

calculated as: [1 – (sample absorbance / blank absorbance)] × 100. Results were expressed as IC_{50} (μg/mL), defined as the concentration required to scavenge 50% of DPPH radicals.

Oxygen radical absorbance capacity (ORAC)

The ORAC assay was performed as described in a previous study [36], with minor modifications. All reagents and samples were prepared in 75 mM phosphate buffer (pH 7.0). In a black 96-well plate, 50 μL of 3 μM fluorescein sodium salt and 50 μL of sample were added and pre-incubated at 37 °C for 15 min in the dark. Oxidation was initiated by adding 25 μL of 221 mM AAPH (Thermo Scientific, Waltham, MA, USA). Fluorescence was measured at excitation/emission wavelengths of 485/535 nm at 1-min intervals for 90 min using a microplate reader. Trolox (10–50 μM) was used as the standard. ORAC values were calculated based on the net area under the fluorescence decay curve (AUC) and expressed as μM TE per mg of dry weight.

Cell culture

C2C12 mouse myoblasts were obtained from ATCC (Manassas, VA, USA) and routinely cultured in DMEM supplemented with 10% FBS and 1% penicillin–streptomycin. Cells were maintained at 37 °C in a humidified atmosphere containing 5% CO_2. For routine passaging, cultures were rinsed with DPBS and detached using 0.05% trypsin for approximately 2 min. The detached cells were reseeded onto 100-mm culture dishes at an initial density of 3×10^5 cells per dish and expanded in growth medium for 48 h.

Dexamethasone-induced C2C12 myotube atrophy model

To establish the dexamethasone-induced myotube atrophy model, C2C12 mouse myoblasts were cultured as described in the "Cell culture" section. Myoblasts were seeded into appropriate culture plates at a density optimized for differentiation. When the cells reached approximately 80%–90% confluence, the growth medium was replaced with differentiation medium consisting of DMEM supplemented with 2% HS and 1% penicillin–streptomycin. The cells were then allowed to differentiate into multinucleated myotubes for 72 h according to a well-established protocol [11, 25].

Following complete differentiation, the mature C2C12 myotubes were pretreated with either ADL crude extract or its fractions at various concentrations for 24 h. Muscle atrophy was subsequently induced by exposing the pretreated myotubes to 10 μM dexamethasone for an additional 24 h. Dexamethasone was prepared by diluting a stock solution in DM to the desired working concentration. All experimental incubations were performed at 37 °C in a humidified atmosphere containing 5% CO_2, consistent with standard cell culture conditions.

This sequential treatment strategy, consisting of pretreatment with test compounds prior to dexamethasone exposure, is a well-established approach for evaluating protective effects against glucocorticoid-induced muscle atrophy in C2C12 myotubes, and was applied in the present study with minor modifications based on previous studies [11, 16, 25].

Cell cytotoxicity

Cell viability was assessed using the MTT assay. Differentiated C2C12 myotubes were treated according to the experimental design described above. Following treatment, 20 μL of MTT solution (0.1%, prepared in DPBS) was added to each well and incubated for 4 h at 37 °C. The supernatant was carefully removed, and the resulting formazan crystals were dissolved in 200 μL of DMSO. Absorbance was measured at 570 nm using a microplate reader (SpectraMax® M2, Molecular Devices, San Jose, CA, USA). Cell viability values above 80% were considered indicative of non-cytotoxicity.

Reactive oxygen species measurement

Intracellular ROS levels were measured using the cell-permeable fluorogenic dye CM-H2DCFDA (Invitrogen, Carlsbad, CA, USA). C2C12 myoblasts were seeded in clear-bottom black 96-well plates at a density of 1×10^4 cells per well, differentiated for 72 h, and treated according to the atrophy model described above. After treatment, the cells were washed with DPBS and incubated with 10 μM CM-H2DCFDA for 30 min at 37 °C in the dark. Following incubation, the cells were washed with DPBS to remove excess dye. Fluorescence intensity was measured at Ex/Em 492/522 nm using a microplate reader. ROS levels were expressed as a percentage relative to the DEX-treated control group [16].

Immunofluorescence staining and image analysis

Cells were seeded in 12-well plates at a density of 7.5×10^4 cells per well and processed for immunofluorescence following completion of the atrophy protocol. Cultures were fixed with 4% paraformaldehyde for 30 min, blocked with 3% bovine serum albumin (BSA) for 1 h, and incubated overnight at 4°C with Alexa Fluor 488-conjugated anti-myosin heavy chain antibody (MF20, 1:100; Invitrogen). Nuclei were counterstained with DAPI (1:5000; Invitrogen). Images were acquired using an inverted fluorescence microscope (Axio Vert.A1, Carl Zeiss). For quantitative analysis of myotube atrophy, the diameters of 50 randomly selected myotubes were measured per treatment group in each biological replicate using ImageJ software resulting in a total of 150 myotubes per treatment group across three independent biological

experiments. The diameter of each myotube was measured at three distinct points along its length, and the mean value was used for statistical analysis.

Western blot analysis

Following completion of the atrophy protocol, myotubes were harvested on day 5. Cell pellets were lysed in RIPA buffer containing protease and phosphatase inhibitors, and protein concentrations were determined using a BCA assay. Equal amounts of protein (20 μg) were separated by SDS–PAGE and transferred onto polyvinylidene fluoride (PVDF) membranes. Membranes were blocked with 5% BSA in TBST and incubated overnight at 4 °C with primary antibodies against MuRF1 and MAFbx (each 1:1000), as well as α-tubulin (1:3000). After washing, membranes were incubated with HRP-conjugated secondary antibodies (1:5000). Protein bands were visualized using ECL and quantified with ImageQuant TL software (v10.2) after imaging on an Amersham ImageQuant 800 system (Cytiva). α-Tubulin was used as the loading control, and the expression levels of target proteins were normalized to α-tubulin.

LC–MS/MS analysis

The phytochemical profiles of ADL and its fractions were characterized using a UHPLC–Orbitrap MS/MS platform. Analyses were performed on a Vanquish ultra-high-performance liquid chromatography (UHPLC) system equipped with a diode-array detector (Thermo Fisher Scientific, Waltham, MA, USA) and coupled to a Q Exactive Orbitrap mass spectrometer fitted with a heated electrospray ionization (HESI) source. Chromatographic separation was carried out on a Hypersil GOLD aQ C18 column (100 × 2.1 mm, 1.9 μm) maintained at 36 °C. The mobile phases consisted of solvent A (0.1% formic acid in water) and solvent B (0.1% formic acid in acetonitrile). The gradient elution program was as follows: 0–3 min, 5% B; 3–14 min, 5–100% B; 14–17 min, 100% B; 17–17.5 min, 100–5% B; and 17.5–21 min, 5% B for column re-equilibration. The flow rate was 0.30 mL/min, and the injection volume was 5 μL. Prior to analysis, all samples were filtered through 0.2 μm PVDF syringe filters.

Data processing and statistical analysis

LC–MS/MS data for ADL and its fractions were processed using Compound Discoverer software (version 3.3, Thermo Fisher Scientific, USA). The following parameters were applied: precursor mass range of 100–1500 Da, retention time window of 0–14 min, alignment mass tolerance of 5 ppm, and minimum peak intensity of 1×10^7. The resulting feature table was exported for heat map visualization and multivariate statistical analyses using SIMCA (version 18.0, Umetrics, Umeå, Sweden), including PCA. Group discrimination was further evaluated using OPLS-DA. Metabolites contributing significantly to group separation were identified based on VIP ≥ 1.5 and $p(\text{corr}) \geq 0.95$. All additional statistical analyses were performed using SPSS (version 12.0, IBM, Armonk, NY, USA). Differences among groups were assessed by one-way analysis of variance (ANOVA) followed by Duncan's multiple range test. Statistical significance was defined as $p < 0.05$. All quantitative data are presented as the mean ± SD from three independent experiments. Cell-based assays, including cell viability, ROS measurement, immunofluorescence-based myotube diameter analysis, and western blot analysis, were performed using three independent biological replicates. For LC–MS/MS metabolite profiling, six biological replicate samples per group or fraction were analyzed.

Metabolite identification

The major metabolites present in the ADL and its fractions were identified by LC–MS/MS using Compound Discoverer 3.3.3 software. An intensity threshold of $\geq 1 \times 10^7$ was applied across all samples. Metabolite annotation was refined by examining MS/MS fragmentation patterns and comparing them with reference spectra and information from mzCloud, PubChem, the MassBank of North America, and relevant published literature.

Abbreviations

ADL	Aruncus dioicus leaf extract
AAPH	2,2′-azobis(2-amidinopropane) dihydrochloride
Akt	Protein kinase B
AMPK	AMP-activated protein kinase
AUC	Area under the curve
BCA	Bicinchoninic acid
BSA	Bovine serum albumin
CM-H2DCFDA	5-(and-6)-chloromethyl-2′,7′-dichlorodihydrofluorescein diacetate
DAPI	4′,6-diamidino-2-phenylindole
DEX	Dexamethasone
DMEM	Dulbecco's modified eagle medium
DMSO	Dimethyl sulfoxide
DPBS	Dulbecco's phosphate-buffered saline
DPPH	2,2-diphenyl-1-picrylhydrazyl
ECL	Enhanced chemiluminescence
F1	Fraction 1 of Aruncus dioicus leaf extract
F2	Fraction 2 of Aruncus dioicus leaf extract
FBS	Fetal bovine serum
FoxO	Forkhead box O
GAE	Gallic acid equivalents
HESI	Heated electrospray ionization
HPLC	High-performance liquid chromatography
HRP	Horseradish peroxidase
HS	Horse serum
IC_{50}	Half-maximal inhibitory concentration
IGF-1	Insulin-like growth factor 1
MAFbx	Muscle atrophy F-box
mTOR	Mechanistic target of rapamycin
MTT	3-(4,5-dimethylthiazol-2-yl)-2,5-diphenyltetrazolium bromide
MuRF1	Muscle RING finger 1
Nrf2/HO-1	Nuclear factor erythroid 2-related factor 2/heme oxygenase-1
OPLS-DA	Orthogonal partial least squares–discriminant analysis

ORAC	Oxygen radical absorbance capacity
PCA	Principal component analysis
PI3K	Phosphoinositide 3-kinase
PVDF	Polyvinylidene fluoride
QE	Quercetin equivalents
ROS	Reactive oxygen species
SIRT1	Sirtuin 1
SPSS	Statistical Package for the Social Sciences
TE	Trolox equivalents
TFC	total flavonoid content
TPC	total phenolic content
UHPLC	ultra-high-performance liquid chromatography
UPS	ubiquitin–proteasome system
VIP	variable importance in projection

Acknowledgements
We thank the BT research facility center, Chung-Ang University.

Author contributions
KBK and JHA conceived and designed the experiments; KBK performed the experiments; KBK and JHA analyzed the data and wrote the manuscript.

Funding
This research was supported by a Chung-Ang University Graduate Research Scholarship (Academic scholarship for College of Biotechnology and Natural Resources).

Data availability
All data generated or analyzed during this study are included in this published article.

Declarations

Competing interests
The authors declare that they have no competing interests.

Received: 15 March 2026 / Accepted: 8 June 2026
Published online: 24 June 2026

References

1. Lee JY, Park J-Y, Seo HT, Seong H-A, Ji Y-J, Lee SE, Seo KH, Kim HD (2020) Samnamul (shoots of *Aruncus dioicus*) inhibit adipogenesis by downregulating adipocyte-specific transcription factors in 3T3-L1 adipocytes. Processes 8:1576
2. Kim J-I, Yun J-A, Jeong Y-K, Baek H-J (2018) Hypoglycemic and hypolipidemic effects of samnamul (shoot of *Aruncus dioicus* var. *kamtschaticus* Hara) in mice fed a high-fat/high-sucrose diet. Food Sci Biotechnol 27:1467–1473
3. Dorjsembe B, Joo H, Nho C, Ham J, Kim J-C (2022) *Aruncus dioicus* var. *kamtschaticus* extract ameliorates psoriasis-like skin inflammation via Akt/mTOR and JAK2/STAT3 signaling pathways in a murine model. Nutrients 14:5094
4. Bowen TS, Schuler G, Adams V (2015) Skeletal muscle wasting in cachexia and sarcopenia: molecular pathophysiology and impact of exercise training. J Cachexia Sarcopenia Muscle 6:197–207
5. Bodine SC, Baehr LM (2014) Skeletal muscle atrophy and the E3 ubiquitin ligases MuRF1 and MAFbx/atrogin-1. Am J Physiol Endocrinol Metab 307:E469–E484
6. Gao Y, Arfat Y, Wang H, Goswami N (2018) Muscle atrophy induced by mechanical unloading: mechanisms and potential countermeasures. Front Physiol 9:235
7. Powers SK, Kavazis AN, McClung JM (2007) Oxidative stress and disuse muscle atrophy. J Appl Physiol 102:2389–2397
8. Schakman O, Kalista S, Barbé C, Loumaye A, Thissen J-P (2013) Glucocorticoid-induced skeletal muscle atrophy. Int J Biochem Cell Biol 45:2163–2172
9. Lee H-J, Kim D, Do K, Yang C-B, Jeon S-W, Jang A (2024) Effects of horse meat hydrolysate on oxidative stress, proinflammatory cytokines, and the ubiquitin-proteasomal system of C2C12 cells. Food Sci Anim Resour 44:132
10. Yamada T, Ashida Y, Tatebayashi D, Himori K (2019) Myofibrillar function differs markedly between denervated and dexamethasone-treated rat skeletal muscles: role of mechanical load. PLoS ONE 14:e0223551
11. Md. Mizanur Rahman AU, Moriwaki H, Yasukawa Y, Uchida T, Takeshi Nikawa (2024) Muscle-protective effect of carnosine against dexamethasone-induced muscle atrophy in C2C12 myotube. J Nutr Sci Vitaminol 70:219–227
12. Tarantino G, Sinatti G, Citro V, Santini SJ, Balsano C (2023) Sarcopenia, a condition shared by various diseases: can we alleviate or delay the progression? Intern Emerg Med 18:1887–1895
13. Nikawa T, Ulla A, Sakakibara I (2021) Polyphenols and their effects on muscle atrophy and muscle health. Molecules 26:4887
14. Kim C, Hwang J-K (2020) Flavonoids: nutraceutical potential for counteracting muscle atrophy. Food Sci Biotechnol 29:1619–1640
15. López-Alarcón C, Denicola A (2013) Evaluating the antioxidant capacity of natural products: a review on chemical and cellular-based assays. Anal Chim Acta 763:1–10
16. Lee H, Kim YI, Kim MJ, Hahm J-H, Seo HD, Ha TY, Jung CH, Ahn J (2022) Castor oil plant (*Ricinus communis* L.) leaves improve dexamethasone-induced muscle atrophy via Nrf2 activation. Front Pharmacol 13:891762
17. Chen C, Yang J-S, Lu C-C, Chiu Y-J, Chen H-C, Chung M-I, Wu Y-T, Chen F-A (2020) Effect of quercetin on dexamethasone-induced C2C12 skeletal muscle cell injury. Molecules 25:3267
18. Yoshioka Y, Imi Y, Kawabata K, Shibata K, Terao J, Miyoshi N (2023) Theophylline prevents dexamethasone-induced atrophy in C2C12 myotubes. J Nutr Sci Vitaminol 69:284–291
19. Hur H, Kim H-J, Lee D, Jo C (2024) Beef peptides mitigate skeletal muscle atrophy in C2C12 myotubes through protein degradation, protein synthesis, and the oxidative stress pathway. Food Funct 15:4564–4574
20. Hah Y-S, Lee WK, Lee S-J, Lee SY, Seo J-H, Kim EJ, Choe Y-I, Kim SG, Yoo J-I (2023) Rutin prevents dexamethasone-induced muscle loss in C2C12 myotube and mouse model by controlling FOXO3-dependent signaling. Antioxidants 12:639
21. Sakuma K, Aoi W, Yamaguchi A (2014) The intriguing regulators of muscle mass in sarcopenia and muscular dystrophy. Front Aging Neurosci 6:230
22. Wing SS, Lecker SH, Jagoe RT (2011) Proteolysis in illness-associated skeletal muscle atrophy: from pathways to networks. Crit Rev Clin Lab Sci 48:49–70
23. Ulla A, Uchida T, Miki Y, Sugiura K, Higashitani A, Kobayashi T, Ohno A, Nakao R, Hirasaka K, Sakakibara I (2021) Morin attenuates dexamethasone-mediated oxidative stress and atrophy in mouse C2C12 skeletal myotubes. Arch Biochem Biophys 704:108873
24. Huang Y, Chen K, Ren Q, Yi L, Zhu J, Zhang Q, Mi M (2018) Dihydromyricetin attenuates dexamethasone-induced muscle atrophy by improving mitochondrial function via the PGC-1α pathway. Cell Physiol Biochem 49:758–779
25. Ulla A, Rahman MM, Uchida T, Kayaki H, Nishitani Y, Yoshino S, Kuwahara H, Nikawa T (2024) 3-(4-Hydroxy-3-methoxyphenyl)propionic acid mitigates dexamethasone-induced muscle atrophy by attenuating Atrogin-1 and MuRF-1 expression in mouse C2C12 skeletal myotubes. J Clin Biochem Nutr 76:16
26. Shen Y, Zhang Q, Huang Z, Zhu J, Qiu J, Ma W, Yang X, Ding F, Sun H (2020) Isoquercitrin delays denervated soleus muscle atrophy by inhibiting oxidative stress and inflammation. Front Physiol 11:988
27. Otsuka Y, Egawa K, Kanzaki N, Izumo T, Rogi T, Shibata H (2019) Quercetin glycosides prevent dexamethasone-induced muscle atrophy in mice. Biochem Biophys Rep 18:100618
28. Zhang M, Chang G, Gao S, Wei J, Chen M, Song L, Lu J, Sheng J, Ma X (2024) Kaempferol protects against dexamethasone-induced muscle atrophy in mice by increasing PI3K/AKT/mTOR and NRF2/HO-1/KEAP1 signaling pathways: network pharmacology, molecular docking, and experimental validation studies. Food Sci Hum Wellness
29. Yoon YE, Ju SH, Kim Y, Lee S-J (2025) Natural flavonoids for the prevention of sarcopenia: therapeutic potential and mechanisms. Int J Mol Sci 26:7458
30. Goto T, Teraminami A, Lee J-Y, Ohyama K, Funakoshi K, Kim Y-I, Hirai S, Uemura T, Yu R, Takahashi N (2012) Tiliroside, a glycosidic flavonoid, ameliorates obesity-induced metabolic disorders via activation of adiponectin signaling followed by enhancement of fatty acid oxidation in liver and skeletal muscle in obese-diabetic mice. J Nutr Biochem 23:768–776
31. Hufnagel M, Rademaekers A, Weisert A, Häberlein H, Franken S (2024) Pharmacological profile of dicaffeoylquinic acids and their role in the treatment of respiratory diseases. Front Pharmacol 15:1371613
32. Liu X, Liu M (2022) Chlorogenic acid improves diabetes-associated muscular atrophy in mice. Acta Pol Pharm 79:671–677
33. Singleton VL, Rossi JA (1965) Colorimetry of total phenolics with phosphomolybdic-phosphotungstic acid reagents. Am J Enol Vitic 16:144–158
34. Alzand KI, Mohamed MA (2012) Flavonoids: chemistry, biochemistry and antioxidant activity. J Pharm Res 5:37

35. Marinova G, Batchvarov V (2011) Evaluation of the methods for determination of the free radical scavenging activity by DPPH. Bulg J Agric Sci 17:11–24
36. Huang D, Ou B, Prior RL (2005) The chemistry behind antioxidant capacity assays. J Agric Food Chem 53:1841–1856

Publisher's note

Springer Nature remains neutral with regard to jurisdictional claims in published maps and institutional affiliations.